Mechanical properties and electrochemical behavior of borosilicate glass system

A. Hefnawy[a,c] , N. Elkhoshkhany[b,c,*], F. Mahgoub[c], M. Hussein[c]
[a]*Department of Chemistry, College of Science, University of Bahrain, Sakhir 32038, Kingdom of Bahrain*
[b]*Physics Dept., College of Arts and Sciences at Tabrjal, Jouf University, Al-Jouf, Saudi Arabia*
[c]*Department of Materials Science, Institute of Graduate Studies and Research, Alexandria University, 163 Horreya Avenue, Shatby 21526, Egypt*

New synthesized borosilicate glass system within the molar percentages 50 B_2O_3 – (14–X) SiO_2 – (20+X) Li_2O –15 Na_2O –1Al_2O_3 with X=0, 1, 2, 3, 4, 5 mol % was investigated. The amorphous identity of the samples has been checked by X-ray diffraction (XRD). The decrease of the molar volume (V_m) with increasing Li_2O amount led to an increase in the calculated oxygen packing density (O.P.D). The packing density of the specimens increased also with the inclusion of Li_2O. The Fourier transform infrared (FTIR) showed the transformation of BO_3 to BO_4 units that increased the rigidity of the prepared glass series. The ultrasound wave velocities (longitudinal (v_l) and shear (v_s)) were assigned by the pulse-echo technique. Both (v_l) and (v_s) increased with increasing Li_2O content because of increasing the rigidity of the glass host. The elastic Longitudinal (L), Young's (E), Bulk (B) and Shear (S) moduli besides the Micro-hardness (H) were calculated and all increased with increasing Li_2O content. Ultrasonic mean velocity (v_{mean}) and softening temperature (T_{sm}) increased while Poisson's ratio (σ_m) decreased with the same gradient of X. The theoretical model proposed by (Makishima-Mackenzie) and bond compression model were employed for the prepared glasses. The results from both models showed correspondence with the experimentally obtained values. The impedance spectroscopy was applied to investigate the electrochemical mode of the present glass system and to measure the conductance for all the system samples.

(Received February 5, 2021; Accepted April 13, 2021)

Keywords: Borosilicate glass, FTIR, Mechanical properties, EIS

1. Introduction

Silicate-based glasses have excellent stability properties that make them applicable in advanced fields like semiconductors and electronics. On the other side, B_2O_3 is one of the most stable glass formers that is mainly optical material can used in making dielectric and insulating materials. The mixing between SiO_2 and B_2O_3 to produce borosilicate glasses is of technical and scientific attention because of their minor thermal expansion and hence their resistant to thermal shocks and their broad range of commercial applications. The spread of acoustic waves in the bulk glasses has the importance of understanding the mechanical features, where this can give information about the microstructure and the dynamics of the glasses [1-3]. Many authors have surveyed the structural and the mechanical properties of borosilicate glass, by virtue of its various physical and chemical properties and broad range of uses which include: pharmaceuticals industry, industrial chemical process plants, laboratories, bulbs for high powered lamps, domestic kitchens and in the semiconductor industry through the evolution of micro electro-mechanical systems (MEMS) [4, 5]. Also the properties of the borosilicate glasses through adding several alkali oxides as Li_2O and Na_2O (as a glass modifier) and adding Al_2O_3 oxide (as a conditional glass former) to B_2O_3 and SiO_2 oxides. It was found that the inclusion of Li_2O breaks Si–O–Si linkage and promotes the general mechanical properties [3, 4].

This paper aims to study the mechanical and the electrochemical properties of 50 B_2O_3 – (14–X) SiO_2 – (20+X) Li_2O –15 Na_2O –1Al_2O_3 where, X=0, 1, 2, 3, 4, 5 mol % glass system. In addition, to show the influence of adding the Li_2O content and dropping the SiO_2 content on

*Corresponding author: elkhoshkhany@alexu.edu.eg

ultrasound velocities, mechanical behavior and IR spectra, mainly through measuring both the longitudinal and shear velocities [6].

The elastic moduli of the glass can be evaluated based on experimental measurements and theoretically via the models such as Makishima - Mackenzie model or bond compression model [1]. In addition, the electrochemical impedance spectroscopy technique can been applied to check the electrochemical properties and to explore the conductance alongside investigating the corrosion conduct for all glass samples [7, 8].

2. Experimental procedures

2.1. Glass preparation

Preparation of 50 B_2O_3 – (14–X) SiO_2 – (20+X) Li_2O –15 Na_2O –1Al_2O_3, where X=0, 1, 2, 3, 4, 5 mol % borosilicate glass system has been accomplished by melt-quenching technique. In the preparation, high quality powders of boric acid H_3BO_3 (99.98%, Aldrich), acid-washed quartz sands SiO_2 (99.9 %), lithium carbonate Li_2CO_3 (99.5%, EUROMEDEX), sodium carbonate Na_2CO_3 (99%, Chemajet) and aluminum oxide Al_2O_3 (99%, Baraclude) were weighed in compliance with the required quantities using a single digital balance of 0.1 mg accuracy (SHIMADZU AX 200). The batches then mixed using the mortar to produce homogeneous mixtures. After that, the patches were placed in a platinum crucible and entered in an electric oven to procedure homogeneous melts at 1040 ^oC for 20 minutes for each sample. The melts were cast onto a rectangular slab from a preheated stainless-steel mold, which has a diameter of 12 mm and a length of 6 mm, then transferred to the annealing furnace at 400 ^oC for two hours to avert developing the strains through the quenching. After the furnace was shut down, the samples permitted to cool until the room temperature. The surfaces of samples were made as parallel opposite faces by using a lapping machine with 600 grades SiC powder.

2.2. X-ray diffraction characterization (XRD)

X-ray Diffraction (XRD) was used to detect the amorphous mode of glasses [2, 9]. X-ray Diffractometer (PW1700: Philips Eindhoven, the New Netherlands) using CuK as a radiation fountainhead has been used in the characterization of present glass.

2.3. Fourier-transform infrared spectroscopy (FTIR)

FTIR spectroscopy was executed to explore the glass structural units. The Bruker infrared spectrum model Vertex 70V recorded the spectra (KBr Beam Splitter). The samples were well blended with the KBr and pushed to shape transparent pellets, which were used in the test at room temperature in the range 400–2000 cm^{-1} in an absorbance mode [9, 10].

2.4. Physical properties calculations

The density (ρ) of all glass samples was determined using Archimedes Principle through using the toluene as an immersion liquid by the displacement method. For more accuracy, the measurement was remade three times and the density for every sample was measured to the fourth decimal (± 0.0004 g/cm^3). The molar volume (V_m) and Oxygen Packing Density (O.P.D) were calculated then depending on (ρ). Equations for calculating (ρ), (V_m) and (O.P.D) can be found in the reference [11].

2.5. Ultrasonic velocities measurements:

The ultrasonic wave velocities were obtained by using the classical pulse-echo technique at the room temperature by utilizing the use of 2.25 MHz X-cut and Y-cut adapters, and a USM2 (Krautkramer) ultrasonic flaw detector. The velocity ($\boldsymbol{U}$) was determined according to the relation:

$$\boldsymbol{U} = \frac{\boldsymbol{2X}}{\boldsymbol{\Delta t}} \tag{1}$$

where X is the glass thickness and $\boldsymbol{\Delta t}$ is the time spacing.

All velocity measurements were executed at 25 ^{o}C (298 K) at a frequency of 4 MHz with repeating the measurements three times to ensure data accuracy [4]. The estimated error of the velocities measurements is about 0.04%.

2.6. Determination of the elastic moduli

Depending on the longitudinal (v_l), shear velocities (v_s) and (ρ) of each sample, the elastic moduli can be calculated as the following definitions [6].

The Longitudinal Modulus (L):

$$L = \rho {v_l}^2 \tag{2}$$

Shear Modulus (G):

$$G = \rho {v_s}^2 \tag{3}$$

Bulk Modulus (K):

$$K = L - (4/3\ )G \tag{4}$$

Young's Modulus (E):

$$E = 2(1 + \sigma)G \tag{5}$$

Poisson's Ratio (σ):

It is the ratio between the transversal contraction strains to the longitudinal extension strain toward the direction of applied tensile force as given by the relation (6):

$$\sigma = \frac{(\ L - 2G\ )}{2\ (L - G)} \tag{6}$$

Mean sound velocity (v_{mean}):

$$v_{mean} = \left(\frac{\left({}^{1}/_{{v_l}^3} \right) + (1/{v_s}^3)}{3} \right)^{-\frac{1}{3}} \tag{7}$$

Debye temperature (θ_D): Is an experimental parameter in Debye's heat formula, for solids it represents the temperature at which all the vibrational modes are excited. The relation (8) can give it

$$\theta_D = \frac{h}{K_B \left(\frac{9N}{4\pi V} \right)^{\frac{1}{3}}} * v_{mean} \tag{8}$$

Micro-hardness (H_U):

Provide the necessary data about the microstructure and the hardness of the material and can be calculated by the relation (9)

$$\mathrm{Hu} = \frac{(1 - 2\sigma)E}{6(1 + \sigma)} \tag{9}$$

Softening temperature (T_{sm}):

The temperature at which the material softens under a fixed pressure and various standard conditions. It can be given by:

$$T_{sm} = \frac{M.wt.}{\rho C} v_s^2 \quad (10)$$

Acoustic impedance (Z):

Determines the reflection and transmission of the sound energy in the glass and can be obtained by

$$Z = v_{mean}\ \rho \quad (11)$$

Knowing that h is Plank's constant, k_B is Boltzmann constant, N is the number of the vibrating atoms for each unit volume, M.wt. is the molecular weight while C is a constant equal 0.5074×10^5 cm/$k^{1/2}$s.

2.7. Theoretical elastic moduli and Poisson's ratio

2.7.1. Makishima - Mackenzie model

It is a theoretical model that used to compute the elastic moduli (Young's (E_m), bulk (K_m), shear (Gm) moduli, and Poisson's ratio (σm) of the oxide glasses. It mainly depends on both the dissociation energy per unit volume of glasses (G_t) and the packing density (V_t) as the following equations:

$$E_m = 2V_tG_t \quad (12)$$

$$K_m = 5.862\ V_t^2 \sum G_i\ x_i \quad (13)$$

$$G_m = 3E_mK_m/(9K_m - E_m) \quad (14)$$

$$\sigma_m = (E_m/2G_m) - 1 \quad (15)$$

$$G_t = \sum_i (G_i\, x_i) \quad (16)$$

$$V_t = \left(\frac{\rho}{M.wt}\right)\sum V_i\ X_i \quad (17)$$

where, V_i is the packing factor for the oxide. [1, 12-17].

2.7.2. Bond compression model

The conduct of the experimental elastic moduli can interpreted quantitatively by using this model. According to relations (18 - 21) respectively, the average stretching force constant ($\bar{F}$), the number of bonds for each unit volume (n_b), the estimated bulk modulus (K_{bc}), the average atomic ring size of the network (ℓ) were calculated as the following:

$$\bar{F} = \frac{\sum(xn_ff)_i}{\sum(xn_f)_i} \quad (18)$$

$$n_b = (\frac{N_A}{V_M})\sum_i (n_fx)_i \quad (19)$$

$$K_{bc} = \sum (n_b\, r^2F\ /9) \quad (20)$$

$$\ell = \left(0.0106\ \frac{F}{K_e}\right)^{0.26} \quad (21)$$

r is the bond length, f is the stretching force constant of the oxide $= \frac{17}{r_0^2}$, N_A is Avogadro's number, n_f is the coordination number of the cation, and K_e is the experimental bulk modulus [11,14 ,18-22].

Also, the intermediate cross-link density ($\bar{n}_c$), the theoretical Poisson's ratio (σ_{bc}), the calculated shear (G_{bc}), longitudinal (L_{bc}) and Young's (E_{bc}) moduli were calculated from relations (22-26) respectively

$$\bar{n}_c = \frac{\sum_i x_i\,(n_c)_i (N_C)_i}{\sum_i x_i\,(N_c)_i} \tag{22}$$

$$\sigma_{bc} = 0.28(\bar{n}_c)^{-0.25} \tag{23}$$

$$G_{bc} = 1.5\,K_{cal}\left[\frac{1-2\sigma_{bc}}{1+\sigma_{bc}}\right] \tag{24}$$

$$L_{bc} = K_{cal} + 1.33\,G_{bc} \tag{25}$$

$$E_{bc} = 2(1+2\sigma_{bc})G_{bc} \tag{26}$$

where, N_c is the number of cations per glass formula unit [1, 19, 21-22].

2.8. Electrochemical properties of the glass

2.8.1. Impedance spectroscopy

Electrochemical Impedance Spectroscopy (EIS) commonly used to investigate the electrochemical parameters for the interface systems. The Impedance (Z) can be illustrated in the form of Nyquist diagram, which is a relation between the real (Z_{real}) and the imaginary parts (Z_{imag}), and hence each point corresponds to an unlike frequency from the other [23]. (EIS) was performed for the samples by the two-electrode method by using a Gamry PCI4G750 Potentiostat/Galvanostat/ZRA analyzer, with a Gamry framework system based on ESA400. EIS300 software for EIS measurements and Echem Analyst 5.5 software for the results plotting, graphing, data fitting and calculating were used. The samples were coated by applying carbon paste as an electrically conductive material, then dried for one hour at a temperature between 100 - 120 ^{o}C. The samples then held between two parallel surfaces inside the two-electrode cell which connected to Potentiostat in the frequency extent (0.1 Hz - 30kHz) [24, 25].

2.8.2. Conductance measurement

Studying the conductance is complementary to the electrochemical features of the present glass. The conductance (G) is an expression of the ease with which electrical current fluxes through the material. (G) of the samples was determined using HIOKI 3532-50 LCR HITESTER by applying DC current across two electrodes at the frequency limits (50 Hz–5 MHz) [26, 27]. The average conductance (G_{av}) obtained for the glass system has been captured by a personal computer.

3. Results and discussion

3.1. X-ray diffraction

The amorphous essence of the glass series was proved by the nonappearance of any sharp peaks in the XRD spectra as in Fig. 1 [2].

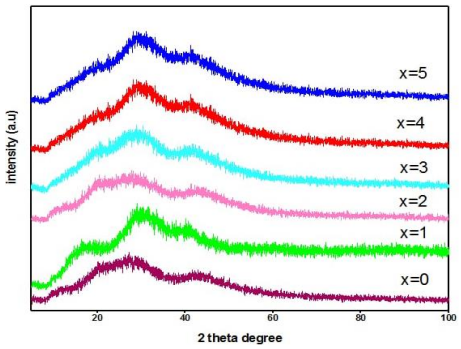

Fig. 1. X-ray Diffract gram of the prepared glass series.

3.2. FTIR spectroscopy

FTIR bands of the glass samples exist in the regions between 400 and 2000 cm^{-1} as in Fig. 2.

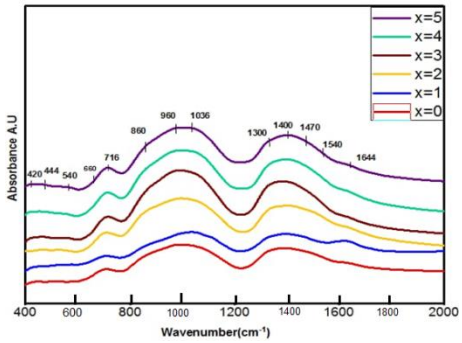

Fig. 2. FTIR Spectra of the prepared glass series.

Notice that the observed FTIR bands of the six samples are similar with a slight shift. The band's wavenumbers and their assignments exhibit the following frequency regions:

1. The bands from 410 to 425 cm^{-1} are due to the stretching vibration of Li–O bonds in the glass network [28].
2. The bands around 444 cm^{-1} are allocated to bending vibration of O–B–O bonds and specific vibration of Na–O bonds [29].
3. The bands from 460 to 540 cm^{-1} are due to bending vibration of Si–O–Si and O–Si–O of bridging oxygen (Q_4) and overlap with B–O–B linkages or Al–O–Al or Al–O–Si bonds. [4, 5, 30].
4. The bands from 650 to 670 cm^{-1} are ascribed to asymmetrical bending vibrations (υ_4) of Si–O–Si bonds [31].
5. The bands from 700 to 720 cm^{-1} are assigned to B–O–B bending vibrations of BO_3 triangles [31].
6. The bands from 840 to 880 cm^{-1} are assigned to stretching vibrations of tri-, tetra-, and penta borate groups [32].
7. The peaks from 930 to 960 cm^{-1} are assigned to the stretching vibrations of B–O bonds in the tetrahedral BO_4 groups. Moreover, to appearance of peaks for stretching vibration of BO_4 units in several structural groups and it is noticed that these peaks shifted to right with the gradient (from X=0 to X=5 mol %) indicating an increase of BO_4 units with the same gradient [4, 5, 31].
8. The bands from 1000 to 1100 cm^{-1} are according to the symmetric stretching vibration of Si-O-Si bonds of [SiO_4] units [4, 5, 31].

9. The broad bands around 1300 cm^{-1} are ascribed to non-bonding oxygen of asymmetric stretching vibrations of BO_3 units from various kinds of borate groups [31].

10. The bands from 1400 to 1500 cm^{-1} are assigned to B–O antisymmetric stretching vibration of triangles BO_3 units only [4,31].

11. The broad bands from 1530 to 1550 cm^{-1} are dedicated to the stretching modes of Si–O and/or B–O bonds of the tetrahedral BO_4 units [33].

12. The bands from 1640 to 1650 cm^{-1} are assigned to the existence of $B–O^-$ bonds in isolated pyroborate groups [31].

3.3. Main physical properties

All (ρ), (V_m) and (O.P.D) for each sample are in Table 1. As displayed by the table, it is clear that the measured (ρ), and (O.P.D) increase with the variability of the mol % (from 0 to 5) of all samples. The densities varied from 2.3787 to 2.3907 (g/cm^3) while the (O.P.D) varied from 0.0863 to 0.0870 ±0.000238 (g/cm^3). This denotes the increase in the number of oxygen atoms per the sample because of the transformation of [BO_3] units into [BO_4] structural units causing more linking in the glass matrix that makes the glass structure more compact and thus increases the glass density. (V_m) decreases from 25.0193 to 24.2622 ± 0.26 (cm^3/mol) due to decreasing the bond length or the interatomic spacing between the atoms which generates compacted glass structure. Values of the average boron-boron separation are found to decrease with the gradient from X=0 to X=5 mol % which indicates the increase in (ρ) and the decrease in (V_m) for the same gradient of the glass system [34].

Table 1. Density (ρ), Molar volume (V_m), Oxygen Packing Density (O.P.D), and the elastic moduli of the existing glass system.

Sample	X=0	X=1	X=2	X=3	X=4	X=5
(ρ) ± 0.0004 (g/cm^3)	2.3787	2.3790	2.3809	2.3821	2.3875	2.3907
V_m ± 0.26 (cm^3/mol)	25.0193	24.8887	24.7426	24.6025	24.4208	24.2622
O.P.D ±0.000238 (mol/cm^3)	0.0863	0.0864	0.0865	0.0866	0.0868	0.0870
Longitudinal velocity (v_l) (m/s)	6146	6821	6900	6979	7017	7060
Shear velocity (v_s) (m/s)	3772	3780	3782	3793	3810	3828
Longitudinal modulus (L) (Gpa)	89.8504	110.6866	113.3527	116.0256	117.5566	119.1592
Shear modulus (G) (Gpa)	33.8437	33.9925	34.0547	34.2715	34.6572	35.0318
Bulk modulus (K) (Gpa)	44.7254	65.3633	67.9465	70.3303	71.3469	72.4502
Poisson's ratio (σ)	0.1979	0.2784	0.2853	0.2904	0.2910	0.2918
Young's modulus (E) (Gpa)	81.0801	86.9112	87.5392	88.4478	89.4828	90.5076
Micro hardness (H_U) (Gpa)	4.7889	4.8296	4.8626	4.8749	5.0221	6.8170
Acoustic Impedence (Z) (×10^{-6} Kg. $m^{-2}.s^{-1}$)	9.9031	10.0176	10.0392	10.0802	10.1489	10.2114
Mean velocity (v_{mean}) (m/s)	4163	4211	4217	4232	4251	4271
Softening temperature (T_s) (K)	693.56	695.87	697.49	697.58	698.65	700.69
Debay Temperature (Θ_D) (K)	569.40	576.91	578.84	581.99	586.09	590.20

3.4. Ultrasonic velocities

Fig. 3 and Table 1 show changing of the longitudinal (v_l) and shear (v_s) ultrasound velocities for all glass samples with (X mol %). (v_l) varies from 6146 to 7060 (m/s) while the (v_s) varies from 3772 to 3828 (m/s) with the gradient from X=0 to X=5 mol %. This means that the alteration in the oxide's contents plays a fundamental role in increasing the wave's propagation through the glass. The ultrasonic velocity increment is linked to the packing density increment consequently the transformation of Boron ions coordination [6]. Because of the observed packing density increment, the rigidness of glass increases with the gradient from X=0 to X=5 mol % by reason of the formation of more bridging oxygen's (BO's) and hence the ultrasonic velocities increase as mentioned [6].

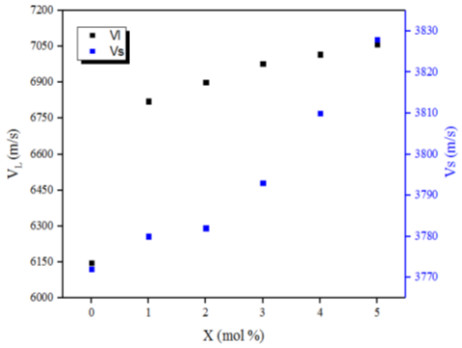

Fig. 3. Variation of longitudinal and shear velocities with the variation of X (mol %) of the prepared glass series.

3.5. Determination of the elastic moduli

Fig. 4 shows variance of elastic moduli with X mol %. The longitudinal modulus (L) varies from 89.8504 to119.1592 GPa, shear modulus (G) varies from 33.8437 to 35.0318 (GPa), bulk modulus (K) varies from 44.7254 to 72.4502 (GPa) while Young's modulus (E) varies from 81.0801 to 90.5076 (GPa) with the gradient from X=0 to X=5 mol % and all results have been shown in Table 1. The elastic moduli increment was a result of increasing the glass rigidity. The rigidity may refer to the creation of (BO's) because of the formation of [BO_4] units within the glass matrix [34]. Increasing the Poisson's ratio (σ) can be taken as evidence for increasing the degree of the cross-linking density of glass network [2]. (σ) That was calculated by relation (6) increases from 0.1979 to 0.2918 (as in Table 1) consistent with the gradient from X=0 to X=5 mol % by reason of the glass network that becomes more tightly packed with the same gradient. As exposed in Table 1, the micro-hardness (H_U) values increase from 4.7889 to 6.8170 (Gpa) while the softening temperature (T_s) increases from 693.56 to 700.69 K. The(H_U) represents the required stress to remove the free volume of the glass while the softening temperature is the temperature point at which the flow changes from viscous to plastic flow and its increasing take as a significance to the invariability of elastic properties. The increase in both(H_U) and (T_s) is ascribed to the increase in glass rigidity [34]. The acoustic impedance (Z) increases from 9.9031 to 10.2114 ($\times 10^{-6}$ Kg. $m^{-2}.s^{-1}$) corresponding to increasing the structure rigidity [6]. The mean sound velocity (υ_{mean}) varies from 4163 to 4271 (m/s) based on reinforcing the glass structure on the grounds of (BO's) creation which leads to increasing the glass rigidity [34]. Debye temperature (Θ_D) increases from 569.40 to 590.20 K and this is due to the generation of stronger rings in the glass system as a result of the creation of (BO's) which denotes increasing the number of the atoms per unit of the glass formula with rising the gradient of X mol % [34]. This result can be confirmed through increasing the number of bonds (as will be discussed in section 3.6.2)

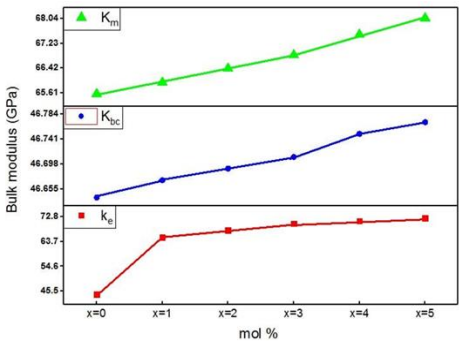

Fig. 4. Variation of Longitudinal (L), shear (G), bulk (K) and Young's (E) moduli Vs. variation of X (mol %) of the prepared glass system.

3.6. Theoretical elastic moduli

3.6.1. Makishima-Mackenzie model

The elastic moduli of the current system by using this model are ordered in Table 2, which show the same trend, and interpretation of the previously calculated experimental elastic moduli as can be noted from the comparison in Fig. 5. As in Table 2, the Young's Modulus (E_m) varies from 41.7735 to 42.8263 (GPa), the bulk modulus (K_m) increases from 65.5812 to 68.0644 (GPa), shear modulus (G_m) varies from 14.9851 to 15.3485 (GPa), while Poisson's ratio (σ_m) varies from 0.3938 to 0.3951. Also, the illustrated results in Table 2 show the increment in the glass packing density (V_t) from 0.5356 to 0.5422 which is related to the decrease in the molar volume (as shown in Table 1) [35]. In the other side, the dissociation energy for each unit volume (G_t) increases from 38.9950 to 39.4900 (KJ/cm^3) with rising X from 0 to 5 (mol %) which confirms the reliance of molar volume on elastic moduli via both (V_t) and (G_t) [35].

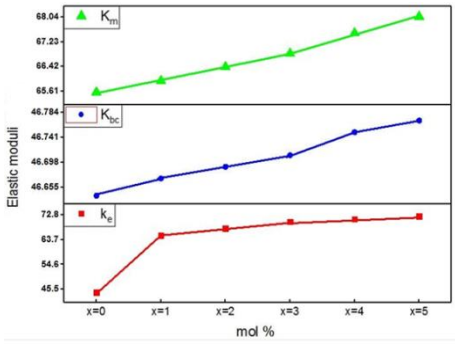

Fig. 5. Comparison between experimental (K_e), Makishima – Mackenzie (K_m) and bond compression (K_{bc}) bulk modulus with variation of X mol % of the prepared glass system.

Table 2. The calculated elastic moduli using Makishima - Mackenzie model for the prepared glass system.

Sample	X=0	X=1	X=2	X=3	X=4	X=5
Packing density (V_t)	0.5356	0.5365	0.5377	0.5387	0.5407	0.5422
The dissociation energy (G_t) KJ/cm^3)	38.9950	39.0940	39.1930	39.2920	39.3910	39.4900
Young's modulus (E_m)	41.7735	41.9455	42.1446	42.3351	42.5996	42.8263
Bulk modulus (K_m)	65.5812	65.9547	66.4143	66.8473	67.5150	68.0644
Shear modulus (G_m)	14.9851	15.0450	15.1139	15.1799	15.2704	15.3485
Poisson's ratio (σ_m)	0.3938	0.3940	0.3942	0.3944	0.3948	0.3951

3.6.2. Bond compression model

The illustrated results in Table 3 show increasing the estimated bulk modulus (k_{bc}) from 46.6453 to 46.7731 (Gpa), shear modulus (G_{bc}) from 27.3687 to 27.5252 (Gpa), longitudinal modulus (L_{bc}) from 83.0456 to 83.3816 (Gpa), Young's modulus (E_{bc}) from 82.6119 to 83.0172 (Gpa), while the theoretical Poisson's ratio (σ_{bc}) varies from 0.2548 to 0.2537. The results show that the elastic moduli of the system (which were studied by bond compression model) have alike trend as that of the previously calculated experimental ones and are compatible with the values that have been calculated by using Makishima - Mackenzie theory as in Fig. 5. The observed increase in (K_{bc}) can be clarified based on the reliance of (K_{bc}) on the number of bonds for each unit volume (n_b) in a direct relation [35]. The gradient of X from 0 to 5 mol % causes (n_b) to increase from 8.4150 to 8.6990 ($m^{-3}\times10^{28}$). This increase of (n_b) is related to the observed increase in mean cross-link density ($\bar{n}_c$) as in Table 3. Also, the rise of ($\bar{n}_c$) denotes increasing the glass rigidity as confirmed from IR spectra analysis because of the generation of rigid [BO_4] units. The ratio (K_{bc}/K_e) is a measure of the extent of the bending bonds that subjected to forming the network bonds. This ratio is supposed to be straightly proportional to the ring diameter (ℓ) and inversely

with the ultrasonic velocities. Decreasing the average ring size (ℓ) from 0.5273 to 0.4615 (nm) (and therefore decreasing (K_{bc}/K_e) ratio values from 1.0429 to 0.6456) is based on increasing the glass connectivity as can be noted from increasing ($\bar{n}_c$) from 1.4624 to 1.4764 which is also approved from decreasing the molar volume as in Table 1. This proves that the structure of the network becomes stiffer and less open as revealed from IR spectra analysis (Fig. 2).

Table 3. The elastic moduli based on the bond compression model of the prepared glass system.

Sample	X=0	X=1	X=2	X=3	X=4	X=5
Average cross-link density per unit formula ($\bar{n}_c$)	1.4624	1.4652	1.4681	1.4709	1.4737	1.4764
The average bond stretching force constant ($\bar{F}$) (N/m)	360.0500	357.8900	355.7300	353.5700	351.4100	349.2500
Number of network bonds per unit volume (n_b) $\times 10^{28}$	8.4150	8.4700	8.5250	8.5810	8.6420	8.6990
The estimated bulk modulus (k_{bc}) (Gpa)	46.6453	46.6685	46.6880	46.7094	46.7540	46.7731
K_{bc}/K_e	1.0429	0.7140	0.6871	0.6641	0.6553	0.6456
The average ring size (ℓ) (nm)	0.5273	0.4771	0.4715	0.4666	0.4641	0.4615
The theoretical Poisson's ratio (σ_{bc})	0.2546	0.2545	0.2544	0.2543	0.2541	0.2540
The calculated shear modulus (G_{bc}) (Gpa)	27.3687	27.3990	27.4269	27.4557	27.4981	27.5252
The calculated longitudinal modulus (L_{bc}) (Gpa)	83.0456	83.1091	83.1658	83.2255	83.3264	83.3816
The calculated Young's modulus (E_{bc}) (Gpa)	82.6119	82.6896	82.7605	82.8340	82.9485	83.0172

3.7. Electrochemical measurements

3.7.1. Impedance spectroscopy measurements

The impedance spectroscopy of the glass series guides to a series of semi-circles in the Nyquist diagram as depicted in Fig. 6 (a-f).

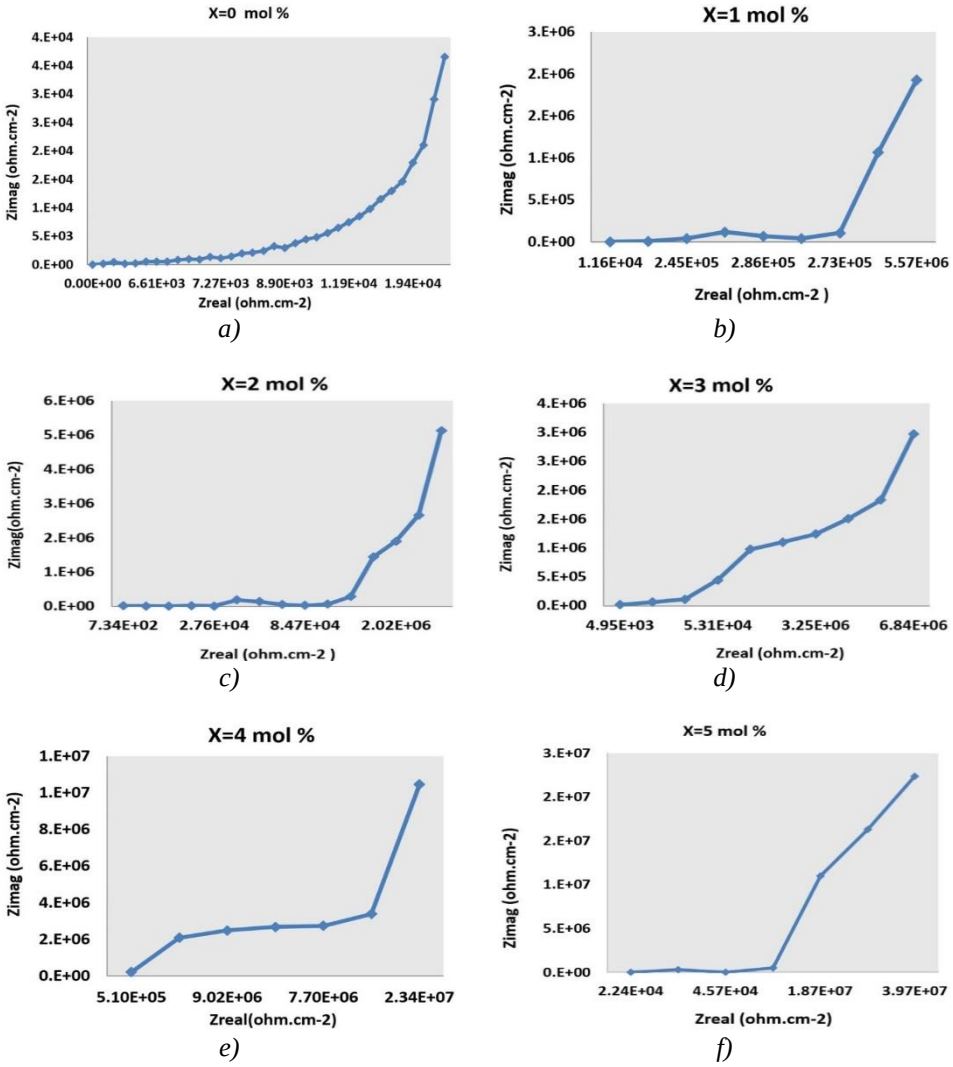

Fig. 6. (a-f) Nyquist plots for the prepared glass system respectively.

It can be noticed from the figure increasing the impedance of the existing glass system with the gradient from X=0 to X=5 mol % which is a result of several reasons:

1- The increase in the O.P.D (As in Table 1) due to increasing the number of oxygen atoms which causes more linkages in the glass network making glass structure more compacted.

2- The increase in the glass density hinders the movement within the glass network, which is accompanied with minimizing (V_m) as in Table 1 [36, 37].

3- Transformation of the triangle boron (BO_3) to the tetrahedral boron (BO_4) which increases the rigidness of the network as deduced from FTIR spectroscopy (Fig. 2) [36].

The polarization resistance used to measure the rates of instantaneous corrosion [38]. The values of polarization resistance (R_p) can be concluded from Fig. 7 through the intersections with the real axis (Z_{real}) [39]. The resulting Nyquist diagram of each sample illustrates that the polarization resistance of impedance increases ascending with the gradient from X=0 to X=5 mol % of the system as recorded in Table 4.

Table 4. The Polarization resistance and average conductance for the prepared glass system.

Sample	Polarization resistance (R_p) $\Omega.cm^2$	Average conductance ($G_{av.}$) Siemens (S) or Ω^{-1}
X=0	3.30×10^{4}	1.74×10^{-4}
X=1	5.57×10^{6}	1.47×10^{-5}
X=2	5.69×10^{6}	9.73×10^{-6}
X=3	6.84×10^{6}	9.58×10^{-6}
X=4	2.34×10^{7}	6.76×10^{-6}
X=5	3.97×10^{7}	6.28×10^{-6}

Values of (R_p) (which have been illustrated in Table 4) vary from 3.30×10^{4} to 3.97×10^{7} ($\Omega.cm^2$). This increase of (R_p) of the impedance emphasizes the existence of an abundance of bond formation and the increase in (BO's) quantum through the appearance of the peaks of stretching vibration of BO_4 with increasing X from 0 to 5 mol% as illustrated in FTIR spectra (Fig. 2). The interstices inside the structure of samples were filled because of the influence of incorporating Li ions in accordance with the same gradient and thus impeding the propagation of more waves within the glass network.

3.7.2. Conductance measurement

The conductance (G) was measured at different frequencies. Values of the average conductance (G_{av}) of each sample have been obtained and results are illustrated in Table 4 which show that (G_{av}) vary from 1.74×10^{-4} to 6.28×10^{-6} (S or Ω^{-1}) for the present glass system. As observed, the conductance reduces with inclusion of Li_2O to the glass system that indicates a drop in the electronic contribution due to the transfiguration in the matrix structure such as creation of (BO's) in the form of BO4 units and generation of several structural oxides as illustrated in FTIR spectroscopy (Fig. 2). These changes cause the intervalence transfer restriction and the electron mobility reduction within the glass network and hence the conductance decreases with the gradient from X=0 to X=5 mol % [40, 41]. Besides that, increased polarization resistance of impedance confirms the interpretation of this decrement in the conductance [37].

4. Conclusions

The glass system within the molar percentages 50 B_2O_3 – (14–X) SiO_2 – (20+X) Li_2O –15 Na_2O –1Al_2O_3, where X=0, 1, 2, 3, 4, 5% has been synthesized and the following consequences have been revealed

1) The longitudinal and shear ultrasound velocities increase based on increasing the packing density and creation of bridging oxygens in the glass system.

2) Increasing the elastic moduli, microhardness, acoustic impedance, expansion coefficient, softening temperature and Debay temperature values of the system confirmed increasing the rigidity of the glass network.

3) Makishima and Mackenzie model and Bond compression model showed that the values of the elastic moduli and Poisson's ratio which have been calculated by using the two models are compatible with the experimental values.

4) Impedance data showed the increase in the polarization resistance of impedance of the glass system on the grounds of increasing the number of the formed bonds within glass structure. The conductance measurements decreased with the gradient from X=0 to X=5 (mol %).

References

[1] Abd El-Moneim, A., A. M. Abd El-Daiem, I. M. Youssof, Phys. Stat. Sol. A **199**, 192 (2003).
[2] K. Sathish, S. Thirumaran, Spectrochim Acta A Mol Biomol Spectrosc **147**, 163 (2015).

[3] A. Abd El-Moneim, Physica B **325**, 319 (2003).
[4] M. S. Gaafara, S. Y. Marzouk, Physica B **388**, 294 (2007).
[5] Yasser B. Saddeek, M. S. Gaafar, Safaa A. Bashier, J Non Cryst Solids **356**, 1089 (2010).
[6] A. N. Kannappan, S. Thirumaran, R. Palani, ARPN Journal of Engineering and Applied Sciences **4**, 27 (2009).
[7] J. Molenda, W. Ojczyk, J. Marzec, J Power Sources **174**, 689 (2007).
[8] R. Keding, C. Rüssel, M. J. Pascual, L. Pascual, A. Durán, J Electroanal Chem **528**, 184 (2002).
[9] J. D. M. Dias, G. H. A. Melo, T. A. Lodi, J. O. Carvalho, P. F. Façanha Filho, M. J. Barboza, A. Steimacher, F. Pedrochi, J Rare Earth **34**, 521 (2016).
[10] D. D. Ramteke, K. Annapurna, V. K. Deshpande, R. S. Gedam, J Rare Earth **32**, 1148 (2014).
[11] N. Elkhoshkhany, Rafik Abbas, R. El-Mallawany, K. S. H. Humoud, Ceram Int **40**, 11985 (2014).
[12] A. Makishima, J. Mackenzie, J Non Cryst Solids **12**, 35 (1973).
[13] Akio Makishima, John D. Mackenzie, J. Non-Cryst. Solids **17**, 147 (1975).
[14] Raouf El-Mallawany, Mater Chem Phys **53**, 93 (1998).
[15] Ulrike Veitn, Christian Rüssel, Ceram Int **42**, 5810 (2016).
[16] Amin Abd El-Moneim, J Fluor Chem **212**, 5 (2018).
[17] A. Abd El-Moneim, I. M. Youssof, L. Abd El-Latif, Acta Mater **54**, 3811 (2006).
[18] E. F. Lambson, G. A. Saunders, B. Bridge, R. A. EL-Mallawany, J Non Cryst Solids **69**, 117 (1984).
[19] Y. B. Saddeek, M. S. Gaafar, N. S. Abd El-Aal, L. Abd El-Latif, Acta Phys Pol A **116**, 211 (2009).
[20] B. Saddeek Yasser, A. Bashier Safaa, Saddek Amr Bakr, Glass Phys Chem **38**, 437 (2012).
[21] M. A. Sidkey, R. E1 Mallawany, R. I. Nakhla, A. Abd E1-Moneim, J Non Cryst Solids **215**, 75 (1997).
[22] A. Abd El-Moneim, L. Abd El-Latif, Phys Chem Glasses **44**, 446 (2003).
[23] S. Lanfredi, A. C. M. Rodrigues, J. Appl. Phys **86**, 2215 (1999).
[24] Shaker A. Ebrahim, Mohamed E. Harb, Moataz M. Soliman, Mazhar B. Tayel, J Taibah Univ Sci **10**, 281 (2016).
[25] Wael I. El Dessouky, Rafik Abbas, Wagih A. Sadik, Abdel Ghaffar M. El Demerdash, Ahmed Hefnawy, Arab J Chem **10**, 368 (2017).
[26] M. Vimalan, A. Ramanand, P. Sagayaraj, Cryst. Res. Technol. **42**, 1091 (2007).
[27] Sagadevan Suresh, Appl Nanosci **4**, 325 (2014).
[28] N. Elkhoshkhanya, Samir Y. Marzouk, Mohamed A. Khattab, Shaimaa A. Dessouki, Mater Charact **144**, 274 (2018).
[29] M. A. Samee, A. Edukondalu, Shaik Kareem Ahmmad, Sair Md. Taqiullah, Syed Rahman, J Electron Mater **42**, 2516 (2013).
[30] Feng He, Caiming Ping, Yuanyuan Zheng, Phys Procedia **48**, 73 (2013).
[31] Priyanka Goyal, Yogesh Kumar Sharma, Sudha Pal, Umesh Chandra Bind, Shu-Chi Huang, Shyan-Lung Chung, J Lumin **192**, 1227 (2017).
[32] Ebtisam Ahmed Saad, Fatma Hatem ElBatal, Amira Mohamed Fayad, Fouad Abbass Moustafa, Silicon **3**, 85 (2011).
[33] T. G. V. M. Rao, A.Rupesh Kumar, N. Veeraiah, M. Rami Reddy, J Phys Chem Solids **74**, 410 (2013).
[34] M. K. Halimah, H. A. A. Sidek, W. M. Daud, H. Zainul, Z. A. Talib, A. W. Zaidan, A. S. Zainal, H. Mansor, Am. J. Appl. Sci **2**, 1541 (2005).
[35] N. Elkhoshkhany, R. El-Mallawany, Eslam Syala, Ceram Int **42**, 19218 (2016).
[36] A. P. Raut, V. K. Deshpande, Mater Res Express **5**, 015201 (2018).
[37] Arthur Ayres Neto, Joana de Noronha Teixeira Mendes, Juliana Maria Gonçalves de Souza, Miguel Redusino Jr., Rodrigo Leandro Bastos Pontes, Mar Georesour Geotec **31**, 125 (2013).
[38] C. Androde, J. A. Gonzhlez, Mater Corros **29**, 515 (1978).
[39] Bing-Ang Mei, Jonathan Lau, Terri Lin, Sarah Tolbert, Bruce Dunn, Laurent Pilon, J Phys Chem C **122**, 24499 (2018).

[40] Doris Ehrt, Ralf Keding, Phys. Chem. Glasses: Eur. J. Glass Sci. Technol. B **50**, 165 (2009).
[41] Hassan M. M. Moawad, Himanshu Jain, Raouf El-Mallawany, Tawfik Ramadan, Mohamed El-Sharbiny, J Am Ceram Soc **85**, 2655 (2002).